AGU100 ADVANCING EARTH AND SPACE SCIENCE

Geophysical Research Letters

RESEARCH LETTER
10.1029/2018GL077880

Key Points:
- The warm ENSO phase exhibits an asymmetry in its predictability limit between the developing and decaying stage
- The asymmetrical inherent predictability limit explains the asymmetry of operational forecast skill for warm ENSO events
- Nonlinear error growth, especially during the first 8-month lead forecasts, contributes to the asymmetry of the predictability limit

Supporting Information:
- Supporting Information S1

Correspondence to:
J. Li and R. Ding,
ljp@bnu.edu.cn;
drq@mail.iap.ac.cn

Citation:
Hou, Z., Li, J., Ding, R., Karamperidou, C., Duan, W., Liu, T., & Feng, J. (2018). Asymmetry of the predictability limit of the warm ENSO phase. *Geophysical Research Letters*, *45*, 7646–7653. https://doi.org/10.1029/2018GL077880

Received 15 MAR 2018
Accepted 21 JUN 2018
Accepted article online 28 JUN 2018
Published online 3 AUG 2018

Asymmetry of the Predictability Limit of the Warm ENSO Phase

Zhaolu Hou[1,2,3], Jianping Li[2,4], Ruiqiang Ding[1,2,3], Christina Karamperidou[5], Wansuo Duan[1,3], Ting Liu[6], and Jie Feng[7]

[1]State Key Laboratory of Numerical Modeling for Atmospheric Sciences and Geophysical Fluid Dynamics (LASG), Institute of Atmospheric Physics, Chinese Academy of Sciences, Beijing, China, [2]Laboratory for Regional Oceanography and Numerical Modeling, Qingdao National Laboratory for Marine Science and Technology, Qingdao, China, [3]College of Earth Science, University of Chinese Academy of Sciences, Beijing, China, [4]State Key Laboratory of Earth Surface Processes and Resource Ecology, and College of Global Change and Earth System Science, Beijing Normal University, Beijing, China, [5]Department of Atmospheric Sciences, University of Hawai'i at Mānoa, Honolulu, HI, USA, [6]State Key Laboratory of Satellite Ocean Environment Dynamics, Second Institute of Oceanography, Hangzhou, China, [7]School of Meteorology, University of Oklahoma, Norman, OK, USA

Abstract A nonlinear local Lyapunov exponent method based on monthly sea surface temperature data is employed to explore the predictability limit of warm El Niño–Southern Oscillation (ENSO) events. Results using observational data show an asymmetry of the predictability limit between the developing and decaying stages of the warm ENSO phase. To wit, predictability of the developing stage of warm ENSO events is found to approach a limit of 10 months, less than that of the mature and decaying stages. This asymmetrical predictability limit is also found in a long climate model simulation and may explain the asymmetry in operational forecast skill of warm ENSO events. Through exploring the error growth rate as represented by nonlinear local Lyapunov exponent and the instantaneous error growth rate, it is shown that error growth, especially during the first 8-month lead forecasts, is the primary contributor to the asymmetry of the predictability limit of warm ENSO events.

Plain Language Summary El Niño events have a characteristic development and decay cycle, whereby most events start developing in late boreal spring, peak in boreal winter, and subsequently decay. Model skill in operational forecasting of El Niño events depends on whether the forecast is done during the developing or decaying stage of the event. This study shows that this asymmetry in forecast skill is associated with an asymmetry in the inherent predictability limits of the developing and decay stages of warm El Niño–Southern Oscillation events. These inherent predictability limits stem from the fact that small perturbations of a dynamical system may grow into large forecast errors after a period of time.

1. Introduction

The El Niño–Southern Oscillation (ENSO), as the prominent coupled ocean-atmosphere phenomenon generated in the tropical Pacific, is associated with irregular variations of atmospheric and oceanic circulation at seasonal time scales (McPhaden et al., 2006; Philander, 1990). Although originating and developing in the tropics, ENSO has widespread impacts on the global climate system, including many extratropical regions (Bradley et al., 1987; Feng & Li, 2011; Rasmusson & Carpenter, 1982; Ropelewski & Halpert, 1989; Trenberth et al., 1998). Thus, seasonal forecast skill over various regions depends critically on ENSO predictions (McPhaden et al., 2006; B. Wang et al., 2009). Consequently, the question, whether ENSO has inherent predictability and how it may manifest in seasonal prediction problems has attracted considerable attention in the ENSO research community.

Depending on one's preferred theoretical model of the ENSO system, its predictability arises from difference sources. Leading theoretical hypotheses for ENSO can be loosely grouped into two types (C. Wang et al., 2016). According to the first hypothesis, El Niño is one phase of a self-sustained, unstable, and naturally oscillatory mode of the coupled ocean-atmosphere system (Münnich et al., 1991; Timmermann & Jin, 2002; Zebiak & Cane, 1987). The initial uncertainty of ENSO state will lead to the separation of the evolutionary trajectories of two initial adjacent states as lead time increases; therefore, ENSO has a predictability limit (PL). According to the second hypothesis, El Niño is a stable (or damped) mode triggered by random atmospheric "noises" (An, 2008; Newman & Sardeshmukh, 2017; Penland & Sardeshmukh, 1995; Stein et al. 2014; Thompson & Battisti, 2000). Thus, stochastic forcing or noise plays an important role in the predictability of ENSO.

Additionally, C. Wang et al. (2016) suggested that ENSO is a combination of the first and second types, as the third type. Under the first ENSO theoretical framework, it is possible to make an effective prediction several years in advance when the initial error of the forecast system is reduced (e.g., D. Chen et al., 2004). Predictability of ENSO is an initial value problem and finally controlled by the error growth rate (EGR) in the specification of initial conditions. Karamperidou et al. (2014) approximated such small error growth in the ENSO system using local Lyapunov exponents (LLEs) in observations and models and showed that ENSO predictability exhibits multidecadal-to-centennial variability in the absence of external forcings. While Karamperidou et al. (2014) focused on multidecadal modulation of intrinsic ENSO predictability and did not investigate the dependence of EGRs on the ENSO stage, other studies have undertaken this task, for example, Cai et al., 2003; Cheng, Tang, Jackson, et al., 2010; Cheng, Tang, Zhou, et al., 2010; Tang & Deng, 2010, 2011. These studies showed that EGRs calculated using singular or breeding vectors during the developing and decaying stage are similar in magnitude and larger than that of the mature stage of warm ENSO events.

However, simple visual inspection of the operational forecast results during the most recent 2015–2016 ENSO event (Figure 1a; obtained by the IRI database at International Research Institute for Climate and Society) indicates that the model spread is larger during the warm ENSO developing stage compared to the decaying stage. To confirm that this is characteristic of warm ENSO events, we calculated the root-mean-square error (RMSE) at 3- and 6-month lead times using the ensemble of Niño 3.4 index forecast results from February 2002 to June 2017 provided by the IRI database and the Kaplan sea surface temperature (SST) data set (Kaplan et al., 1998). We chose four strong El Niño events (2002/2003, 2006/2007, 2009/2010, and 2015/2016) to create a composited RMSE of the Niño 3.4 index at 3- (Figure 1b, green curve) and 6-month lead times (Figure 1b, red curve) from the IRI Multimodel Ensemble. The 3- and 6-month RMSE values evolve consistently. Both are low in the decaying phase of the event and high in the developing stage. In addition, Yu et al. (2009) used the conditional nonlinear optimal perturbation method (Mu & Duan, 2003) to investigate the predictability for El Niño and showed that forecasting El Niño in the decaying phase could be much easier than doing so in the developing phase. All these imply that the forecast skill of the different stages of warm ENSO events is asymmetrical.

Is the above-described asymmetry of ENSO forecast skill due to an asymmetry of the inherent PLs of ENSO? EGRs calculated using singular or breeding vectors cannot indicate quantitatively the length of the ENSO PL. Meanwhile, although dynamical models have advanced greatly (Jin et al., 2008; Latif et al., 1998; Mu & Duan, 2003; Tang & Deng, 2011), they are still limited in their ENSO forecast skill, and using them to perform large sets of reforecast experiments is computationally expensive (Kumar et al., 2017). Therefore, using methods that can determine the ENSO PL based on observed SSTs may prove a useful alternative. For example, Karamperidou et al. (2014) compared ENSO predictability estimates derived using LLEs to that gained from the forecast error growth in hindcast experiments using a global climate model. They found that the difference between derived EGR of LLE and the forecast EGRs varies linearly with forecast lead time, which indicates that the "real" PL may be reasonably approximated by using dynamical systems methods based on SST time series (observed or modeled) and without the need to resort to expensive reforecasts.

An improvement to the above-described method is the nonlinear LLE (NLLE), which has been introduced to study atmospheric and oceanic predictability from weather scale to climate scale (B. Chen et al., 2006; Ding et al., 2008, 2010, 2011, 2017; Hou et al., 2017; Li & Ding, 2013). Li and Ding (2013) studied the temporal-spatial distribution of the SST PLs using the NLLE method with monthly observational SST data. They found that the maximum value of annual mean SST PL appears in the tropical central-eastern Pacific (more than 8 months). However, Li and Ding (2013) did not consider the different stages of ENSO development in their study. The present study aims to fill this gap, by using the NLLE method on observational SST data, as well as on SST output from a long control climate model simulation, to estimate how ENSO PLs depend on the stage of warm-ENSO-event development.

2. Methods and Data

The limit of ENSO predictability due to initial conditions is determined using the NLLE approach. A *n*-dimensional nonlinear dynamical system is described by

$$\frac{\mathrm{d}}{\mathrm{d}t}\mathbf{y} = \mathbf{F}(\mathbf{y}), \tag{1}$$

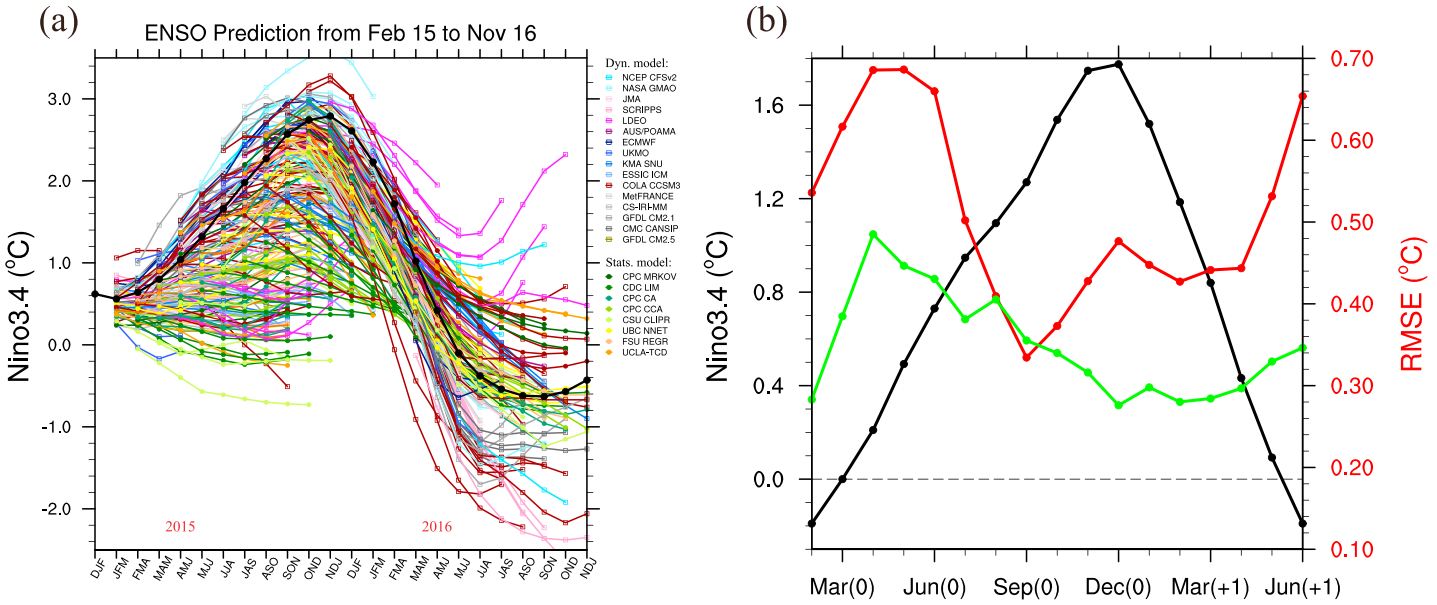

Figure 1. (a) Forecasts of sea surface temperature anomalies for the Niño 3.4 region (5°S–5°N, 170–120°W) with a lead time of 9 months (http://iri.columbia.edu/our-expertise/climate/enso/). (b) Composited root-mean-square error (RMSE) and Niño 3.4 index (black) for four strong El Niño events (2002/2003, 2006/2007, 2009/2010, and 2015/2016). The green (red) curve in (b) represents the RMSE during 3-month (6-month) lead times. ENSO = El Niño–Southern Oscillation.

where $\mathbf{y} = [y_1(t), y_2(t), \ldots\ldots, y_n(t)]^{\mathrm{T}}$ is the state vector at time t, $\mathbf{F}$ denotes the dynamical system and the superscript T represents the transpose. The evolution equation of an error $\boldsymbol{\delta} = [\delta_1(t), \delta_2(t), \ldots\ldots, \delta_n(t)]^{\mathrm{T}}$, superimposed on a state $\mathbf{y}$, is given by

$$\frac{d}{dt}\boldsymbol{\delta} = \mathbf{J}(\mathbf{y})\boldsymbol{\delta} + \mathbf{G}(\mathbf{y}, \boldsymbol{\delta}), \tag{2}$$

where $\mathbf{J}(\mathbf{y})\boldsymbol{\delta}$ are the tangent linear terms of the error $\boldsymbol{\delta}$, and $\mathbf{G}(\mathbf{y}, \boldsymbol{\delta})$ are the nonlinear terms. Without making a linear approximation, solutions of equation (2) can be solved by numerically integration along the reference solution $\mathbf{y}$, that is,

$$\boldsymbol{\delta}(t_i) = \boldsymbol{\eta}(\mathbf{y}(t_0), \boldsymbol{\delta}(t_0), t_i)\boldsymbol{\delta}(t_0), \tag{3}$$

where $\boldsymbol{\eta}(\mathbf{y}(t_0), \boldsymbol{\delta}(t_0), t_i)$ represents the nonlinear propagator. The definition of NLLE is

$$\lambda(\mathbf{y}(t_0), \boldsymbol{\delta}(t_0), t_i) = \frac{1}{t_i - t_0} \ln \frac{\|\boldsymbol{\delta}(t_i)\|}{\|\boldsymbol{\delta}(t_0)\|}, \tag{4}$$

where $\lambda(\mathbf{y}(t_0), \boldsymbol{\delta}(t_0), t_i)$ is the function of the initial state $\mathbf{y}(t_0)$, the initial error $\boldsymbol{\delta}(t_0)$ and time t_i.

For a specific class of states, the ensemble mean NLLE, obtained by averaging $\lambda(\mathbf{y}(t_0), \boldsymbol{\delta}(t_0), t_i)$, can be used to calculate the mean error growth. The method assumes that two state points which have a relatively small initial distance from each other will diverge and, as their trajectories eventually fall into the dynamical system's attractor (Li et al., 2017), they will be indistinguishable from random points. The separation distance, or error, eventually grows to saturation level for a dynamical system (Ding & Li 2007; Li et al., 2017). The error saturation value represents the average distance between two randomly chosen points in the given probability set, implying that once the error growth reaches the saturation level, almost all information on initial states is lost and the prediction becomes meaningless. When the error reaches its saturation value, the PL is reached, and the initial adjacent states drop into the same probability set (attractor; Li et al., 2017). The NLLEs represent the separation rate between the initial adjacent states as the dynamical system evolves, and the PL can be defined by means of the error saturation value. In this study, the 99% percent of the saturation value is used as to define the PL, to reduce the effect of sampling fluctuations. The signal-to-noise ratio is also used to qualitatively verify the potential predictability (Mann & Lees, 1996; Tang et al., 2008).

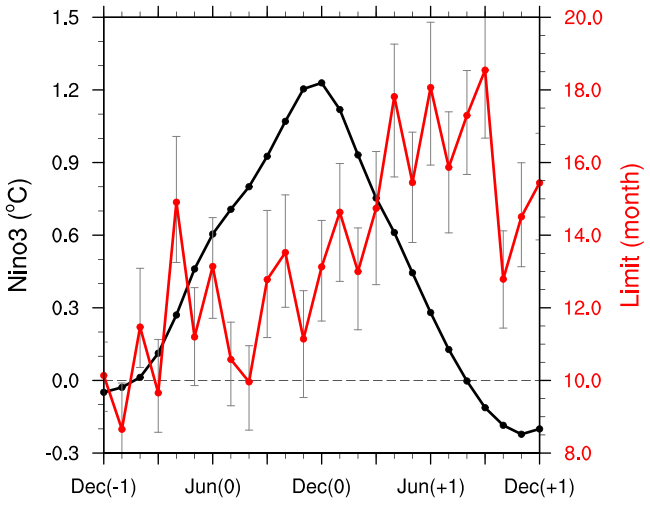

Figure 2. Composited predictability limit (red) of the observed Niño 3 index (black) from 40 warm El Niño–Southern Oscillation events. The gray line gives a level of 90% confidence for the predictability limit of every stage by the bootstrap (resampling) method. The data set used is Kaplan Extended SST V2 (1856–2016).

Based on the observation SST data, the EGR acquired by NLLE merges linear and nonlinear components. The NLLE method has been widely applied to the dynamical systems of ocean and atmosphere and estimated their predictability causing from the uncertainty of initial state, such as Madden-Julian Oscillation (Ding et al., 2010). Thus, we can calculate ENSO PL with NLLE method using observational data in this paper, whether ENSO is chaotic or not.

Monthly mean SST data are used from the Kaplan Extended SST V2 (1856–2016) reconstruction (Kaplan et al., 1998). Lorenz (1969) pointed that finding historical analogues to assess predictability requires a sufficiently long-time series. Li and Ding (2013) indicated that the PL would be undervalued when the observational points are too few to find good local analogues. Karamperidou et al. (2014) also showed that the accuracy of EGRs calculated using a similar method (LLEs) is sensitive to the length of the time series used. The short length of the reconstructed SST data set (161 years; 40 identified ENSO events) may preclude the NLLE method from finding proper analogous trajectories to the reference state. Therefore, 1,280 years of Niño 3 (°S–5°N and 150–90°W) SST anomalies and thermocline depth from a GFDL CM2.1 preindustrial control simulation (Wittenberg, 2009; Wittenberg et al., 2006) are also used in this study to assess the robustness of results. CM2.1 exhibits an irregular ENSO cycle with phase-locking to the boreal winter, albeit with overestimated magnitude, and has been previously used to explore multidecadal-to-centennial modulation of ENSO strength and predictability (Karamperidou et al., 2014; Wittenberg, 2009; Wittenberg et al., 2014). Before calculating the limit, we removed the annual cycle from the SST data and the SST data are smoothed by 3-month running mean.

3. Results

Here the limits of warm ENSO phase predictability are calculated based on the monthly Niño 3 index, smoothed by a 3-month running mean. Warm ENSO events are defined when the December Niño 3 index is greater than 0.5 °C, which takes into account the phase-locking of ENSO to the boreal winter (An & Wang, 2001; Ham & Kug, 2014). The composited PL (Figure 2, red curve) changes during the developing and decaying of ENSO warm anomalies (Figure 2; black curve). In the initial neutral stage, the limit is approximately 10–11 months. The limit has a growing tendency in pace with the warm ENSO phase developing (from December [−1] to December [0]) which lasts until the decaying warm ENSO stage (June–September [+1]). The limit reaches 12 months in the mature warm ENSO phase and 14–15 months in the decaying warm ENSO phase. The difference in PLs between the developing and decaying warm ENSO stage measures up to 4–5 months, which is significant at the 90% level in a bootstrapping test and cannot be explained merely by seasonality in the limit, which is only 2–3 months, as shown in Table 1, a. The difference in predictability found here is confirmed by the signal-to-noise ratio qualitatively (not shown) and is consistent with the variation in model forecast skill across ENSO stages that was shown in Figure 1. Using the Kaplan Extended SST V2 (1950–2016), which has higher quality than before 1950 but includes fewer warm ENSO events, the difference of PL still exists (not shown). In addition, we considered the sensitivity of the PL to the percentage of the

Table 1
Predictability Limit for Different Seasons

	Month											
Predictability limit	January	February	March	April	May	June	July	August	September	October	November	December
(a) From the observed data[a]	14.70	14.91	17.25	15.25	15.75	14.47	14.92	15.57	13.95	13.77	15.09	15.60
(b) From the GFDL CM2.1 simulation[a]	14.83	15.57	17.10	16.15	17.11	16.33	16.03	15.44	15.30	14.97	15.04	15.27

[a]Units (month).

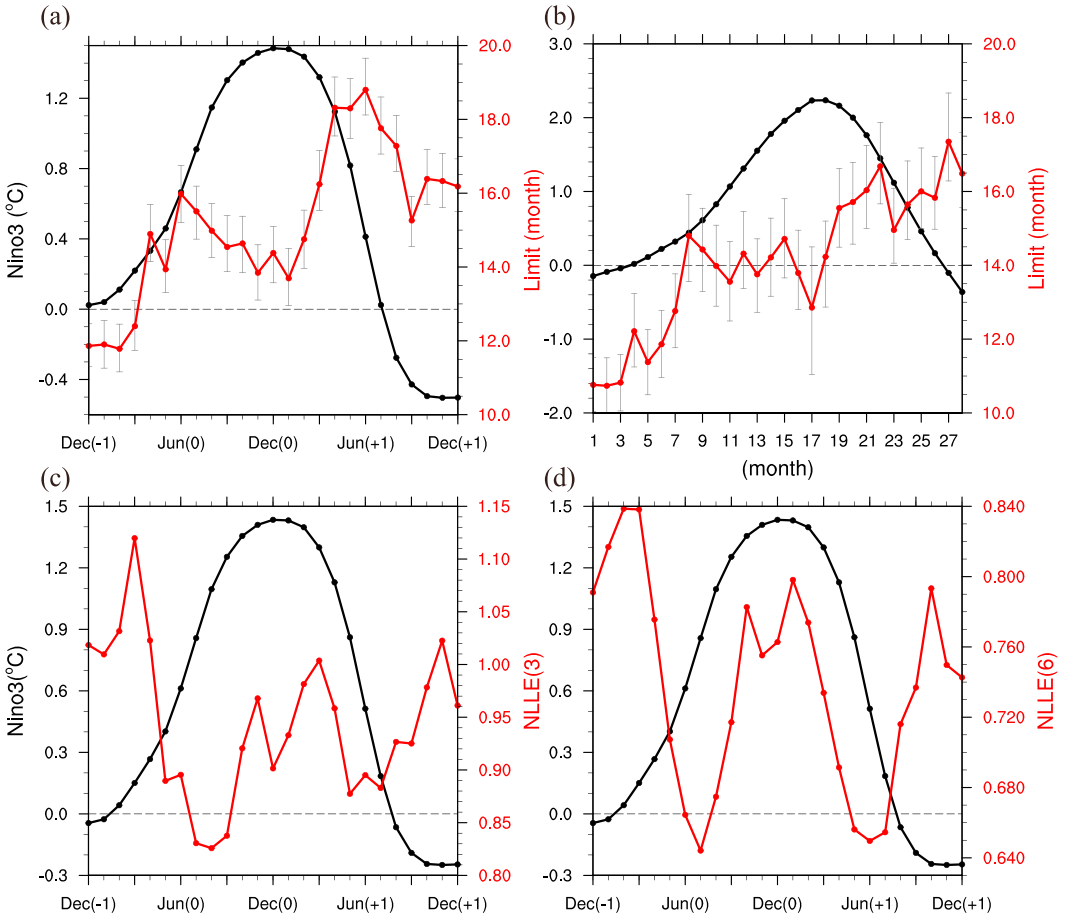

Figure 3. Composited predictability limit (red) as a function of the background warm El Niño–Southern Oscillation event (black) using different composited methods with the 1,280-year monthly Niño index time series from GFDL CM2.1 preindustrial simulation. In (a) the ENSO phase-locking to the boreal winter is considered and the total number of warm ENSO events chosen is 321. (b) The focus is on the ENSO cycle regardless of the month of peak SST anomalies and the number of La Niña to El Niño (El Niño to La Niña) transitions is 114 (136). The gray line gives a level of 90% confidence for the predictability limit of every stage in (a, b). The mean nonlinear local Lyapunov exponent (NLLE; red) spanning 3 (c) and 6 months (d) as a function of the background Niño 3 index (black) shown in (a).

saturation value and confirmed that the asymmetry of PL still exists for saturation values ranging from 80% to 99% (the latter value was used in this study).

As discussed in section 2, the NLLE method is sensitive to the length of the time series used; therefore, we employ the long GFDL CM2.1 simulation to confirm the dependence of ENSO predictability on the stage of development. Indeed, the evolution of the composite PL in 321 events in CM2.1 is similar to the one obtained by observations (cf. Figures 2 and 3a). Note that two warm events spanning two consecutive years are regarded as one warm ENSO event here. Figure 3a shows that the PL in the warm ENSO decaying stage (approximately 16 months) is higher than that in the warm ENSO developing stage (12–13 months). The lowest limit (11–12 months) is found in the neutral stage before the warm developing phase. The PL in different calendar months fluctuates within a range of 1–2 months (Table 1, b); therefore, the differences across calendar months cannot explain the limit differences across the different stages of warm ENSO events. The presence of noise in the observational data set influences the accuracy of estimated PL. However, in a series of experiments adding Gaussian noise at different variance levels, we find that the asymmetry of PL still exists at the 90% significance level (not shown).

To assess whether the method of compositing (based on the magnitude of the Niño 3 index in December) affects the results, we also composited the events around the peak of the full ENSO cycle without regard

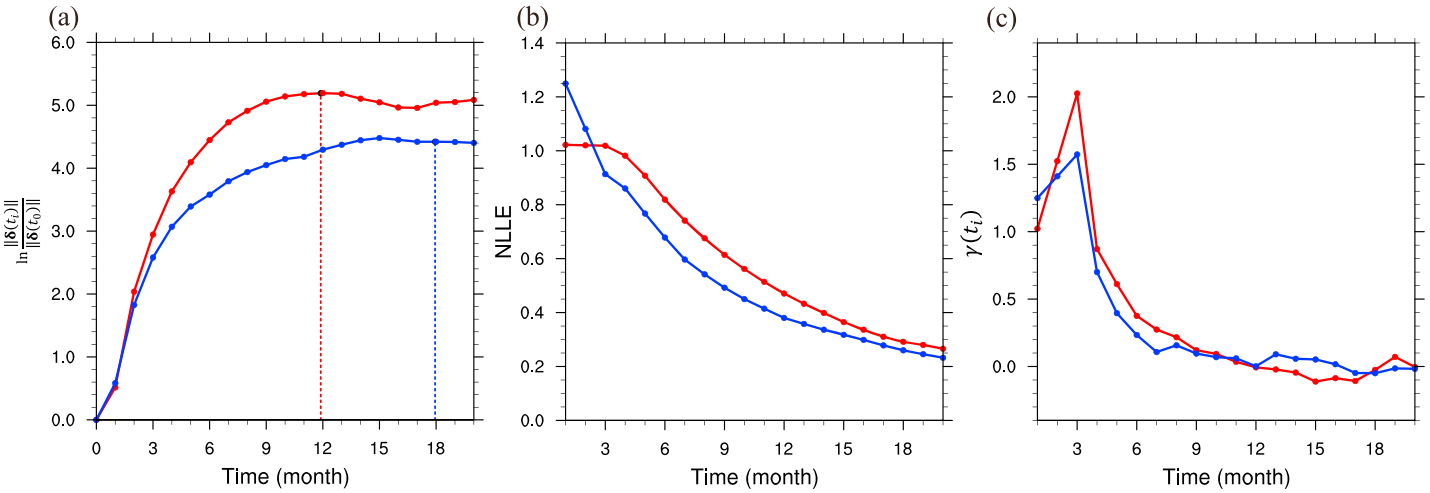

Figure 4. Relative error (a), nonlinear local Lyapunov exponent (NLLE; b) and instantaneous error growth rate $\gamma(t_i)$ in a given month (c) for the developing phase (December [−1] to February [0], red line) and the decaying phase (June [+1] to August [+1], blue line) based on Figure 3a. The vertical red (blue) dashed line in (a) represents the predictability limit of the developing (decaying) phase.

for the month of peak SST anomaly to ensure robustness of the results (see supporting information for details). This alternatively composited Niño 3 index and PL are displayed in Figure 3b. The PL exhibits its highest values in the mature (15–19th month) and decaying phase (22–26th month) compared to the development phase (1–7th month), in agreement with the previous composite (Figure 3a). Here the analogue states in the NLLE method are searched based on the Niño 3 Index time series; using both the Niño 3 Index and the thermocline depth to identify analogical trajectories and calculate the PL yields almost identical results (not shown).

The EGR during the forecast period has a direct effect on the PL (Li & Ding, 2013). Indeed, the average nonlinear error relative growth rates for 3- and 6-month lead times (Figures 3c and 3d) show maximum values when the PL has low values. The NLLEs have the highest values in the neutral stage before the developing stage and are small in the mature and decaying stages of warm ENSO events (Figures 3c and 3d). The characteristics of the limit are already present at NLLEs of a 3-month lead time, which further supports the structure of the PL diagnosed previously.

The PL in the decaying phase of the warm ENSO is longer than that of the developing phase because of the different error growth characteristics. Based on Figure 3a, we selected the period December (−1) to February (0) as the developing stage and June (+1) to August (+1) as the decaying stage. The composited Niño 3 index is 0.06 (0.05) °C and the composited PL is 11.89 (17.94) months for the developing (decaying) stage. Figure 4a exhibits the relative error $\ln\frac{\|\boldsymbol{\delta}(t_i)\|}{\|\boldsymbol{\delta}(t_0)\|}$ for the developing (red line) and decaying (blue line) stages. The relative error in the developing stage is larger than that in the decaying stage. To explain the EGR difference between the two stages, we calculated the NLLE and the instantaneous EGR (γ) in Figure 4a. The NLLE emphasizes the EGR over a period, while the instantaneous EGR $\gamma(t_i)$ gives monthly information and helps identify the key month of growth. The EGR in a given month is defined as follows:

$$\gamma(t_{i+1}) = \frac{1}{t_{i+1} - t_i} \ln\frac{L(t_{i+1})}{L(t_i)}, \tag{5}$$

where i is natural numbers and represents the lead time, $L(t_i)$ is the error between the analogue and reference trajectories at t_i.

The NLLE in the developing stage is larger than that in the decaying stage expect the first 2 months (Figure 4b). This is because the instantaneous EGR in the developing stage is larger in the 2–9th month (Figure 4c). The larger the instantaneous EGR and the NLLE is, the larger the relative error is. From the third to eighth lead month, the γ in the developing stage is larger and the error continually increases faster than

in the decaying stage. The relative error of the developing stage is larger than that of the decaying stage at the same lead month. Thus, the PL of the developing stage is shorter than that of the decaying stage of the warm ENSO event.

4. Conclusions

This study used the NLLE method to provide a quantitative estimate of the PL of the different stages (development, mature, and decaying) of warm ENSO events in observational data and assessed its robustness using a long climate model control simulation. The PL approaches 10 months in the developing stage of warm ENSO events. Meanwhile, the mature and decaying phase have high PL, 13 and 16 months, respectively. The difference in inherent predictability across the different ENSO stages, which is quantified in this study, may explain the asymmetry of ENSO forecast skill by the suite of dynamical and statistical models used for operational ENSO forecasts. We showed that the difference in predictability across ENSO stages is due to the error growth, rather than due to inherent seasonal variations. Here we used the EGR described by NLLE and the instantaneous EGR $\gamma(t_i)$ and showed the impact of lead period on the PL of ENSO, and specifically that error growth mostly contributes to the limit during 8-month lead periods. According to previous studies, the linear EGR, represented by singular values from the tangent linear approximating equation of the ENSO dynamical system (Cheng, Tang, Zhou, et al., 2010), at the decaying stage of the warm ENSO event was equivalent to, or even larger than that at the ENSO developing stage. This could mean that the linear component of the realistic error growth of the ENSO dynamical system cannot explain the PL asymmetry of the warm ENSO. Thus, we hypothesize that the PL asymmetry of warm ENSO events might result from the nonlinear component of the NLLE.

Acknowledgments
This work was jointly supported by the National Natural Science Foundation of China (NSFC) Project (41530424), the NSFC for Excellent Young Scholars (41522502). Ruiqiang Ding is also supported by the National Key Technology Research and Development Program of the Ministry of Science and Technology of China (2015BAC03B07). Wansuo Duan is supported by the National Natural Science Foundation of China (NSFC) Project (41525017). Ting Liu is supported by the National Natural Science Youth Foundation of China (41705049). Christina Karamperidou is supported by U.S. NSF Award AGS-1602097. The Kaplan SST V2 data used in this paper are freely provided by the NOAA/OAR/ESRL PSD, Boulder, Colorado, USA, from their Web site at https://www.esrl.noaa.gov/psd/. The IRI database is available at https://iri.columbia.edu/~forecast/ensofcst/Data/. The GFDL preindustrial control simulation data can be obtained from the GFDL website (http://nomads.gfdl.noaa.gov/CM2.X/CM2.1/available_data.html).

References

An, S. I., & Wang, B. (2001). Mechanisms of locking of the El Niño and La Niña mature phases to boreal winter. *Journal of Climate*, *14*(9), 2164–2176. https://doi.org/10.1175/1520-0442(2001)014<2164:Molote>2.0.Co;2

An, S. I. (2008). Interannual variations of the tropical ocean instability wave and ENSO. *Journal of Climate*, *21*(15), 3680–3686. https://doi.org/10.1175/2008JCLI1701.1

Bradley, R. S., Diaz, H. F., Kiladis, G. N., & Eischeid, J. K. (1987). Enso signal in continental temperature and precipitation records. *Nature*, *327*(6122), 497–501. https://doi.org/10.1038/327497a0

Cai, M., Kalnay, E., & Toth, Z. (2003). Bred vectors of the Zebiak–Cane model and their potential application to ENSO predictions. *Journal of Climate*, *16*(1), 40–56. https://doi.org/10.1175/1520-0442(2003)016<0040:BVOTZC>2.0.CO;2

Chen, B., Li, J., & Ding, R. (2006). Nonlinear local Lyapunov exponent and atmospheric predictability research. *Science in China, Series D: Earth Sciences*, *49*(10), 1111–1120. https://doi.org/10.1007/s11430-006-1111-0

Chen, D., Cane, M. a., Kaplan, A., Zebiak, S. E., & Huang, D. (2004). Predictability of El Niño over the past 148 years. *Nature*, *428*(6984), 733–736. https://doi.org/10.1038/nature02439

Cheng, Y., Tang, Y., Jackson, P., Chen, D., Zhou, X., & Deng, Z. (2010). Further analysis of singular vector and ENSO predictability in the Lamont model–Part II: Singular value and predictability. *Climate Dynamics*, *35*(5), 827–840. https://doi.org/10.1007/s00382-009-0728-z

Cheng, Y., Tang, Y., Zhou, X., Jackson, P., & Chen, D. (2010). Further analysis of singular vector and ENSO predictability in the Lamont model—Part I: Singular vector and the control factors. *Climate Dynamics*, *35*(5), 807–826. https://doi.org/10.1007/s00382-009-0595-7

Ding, R. Q., & Li, J. P. (2007). Nonlinear finite-time Lyapunov exponent and predictability. *Physics Letters, Section A*, *364*(5), 396–400. https://doi.org/10.1016/j.physleta.2006.11.094

Ding, R. Q., Li, J. P., & Ha, K. J. (2008). Trends and interdecadal changes of weather predictability during 1950s–1990s. *Journal of Geophysical Research*, *113*, D24112. https://doi.org/10.1029/2008JD010404

Ding, R. Q., Li, J. P., & Li, B. S. (2017). Determining the spectrum of the nonlinear local Lyapunov exponents in a multidimensional chaotic system. *Advances in Atmospheric Sciences*, *34*(9), 1027–1034. https://doi.org/10.1007/s00376-017-7011-8

Ding, R. Q., Li, J. P., & Seo, K. H. (2010). Predictability of the Madden–Julian Oscillation estimated using observational data. *Monthly Weather Review*, *138*(3), 1004–1013. https://doi.org/10.1175/2009MWR3082.1

Ding, R. Q., Li, J. P., & Seo, K. H. (2011). Estimate of the predictability of boreal summer and winter intraseasonal oscillations from observations. *Monthly Weather Review*, *139*(8), 2421–2438. https://doi.org/10.1175/2011mwr3571.1

Feng, J., & Li, J. (2011). Influence of El Niño Modoki on spring rainfall over south China. *Journal of Geophysical Research*, *116*, D13102. https://doi.org/10.1029/2010JD015160

Ham, Y. G., & Kug, J. S. (2014). ENSO phase-locking to the boreal winter in CMIP3 and CMIP5 models. *Climate Dynamics*, *43*(1–2), 305–318. https://doi.org/10.1007/s00382-014-2064-1

Hou, Z., Li, J., Ding, R., Feng, J., & Duan, W. (2017). The application of nonlinear local Lyapunov vectors to the Zebiak–Cane model and their performance in ensemble prediction. *Climate Dynamics*, *51*(1-2), 283–304. https://doi.org/10.1007/s00382-017-3920-6

Jin, E. K., Kinter, J. L., Wang, B., Park, C. K., Kang, I. S., Kirtman, B. P., & Yamagata, T. (2008). Current status of ENSO prediction skill in coupled ocean-atmosphere models. *Climate Dynamics*, *31*(6), 647–664. https://doi.org/10.1007/s00382-008-0397-3

Kaplan, A., Cane, M. A., Kushnir, Y., Clement, A. C., Blumenthal, M. B., & Rajagopalan, B. (1998). Analyses of global sea surface temperature 1856–1991. *Journal of Geophysical Research*, *103*(C9), 18,567–18,589. https://doi.org/10.1029/97JC01736

Karamperidou, C., Cane, M. A., Lall, U., & Wittenberg, A. T. (2014). Intrinsic modulation of ENSO predictability viewed through a local Lyapunov lens. *Climate Dynamics*, *42*(1–2), 253–270. https://doi.org/10.1007/s00382-013-1759-z

Kumar, A., Hu, Z. Z., Jha, B., & Peng, P. T. (2017). Estimating ENSO predictability based on multi-model hindcasts. *Climate Dynamics*, *48*(1–2), 39–51. https://doi.org/10.1007/s00382-016-3060-4

Latif, M., Anderson, D., Barnett, T., Cane, M., Kleeman, R., Leetmaa, A., & Schneider, E. (1998). A review of the predictability and prediction of ENSO. *Journal of Geophysical Research*, *103*(C7), 14,375–14,393. https://doi.org/10.1029/97JC03413

Li, J. P., & Ding, R. Q. (2013). Temporal-spatial distribution of the predictability limit of monthly sea surface temperature in the global oceans. *International Journal of Climatology*, *33*(8), 1936–1947. https://doi.org/10.1002/joc.3562

Li, J. P., Feng, J., & Ding, R. (2017). Attractor radius and global attractor radius and their application to the quantification of predictability limits. *Climate Dynamics*, 1–16. https://doi.org/10.1007/s00382-017-4017-y

Lorenz, E. N. (1969). Atmospheric predictability as revealed by naturally occurring analogues. *Journal of the Atmospheric Sciences*, *26*, 636–646. https://doi.org/10.1175/1520-0469/(1969)26<636:APARBN>2.0.CO;2

Mann, M. E., & Lees, J. M. (1996). Robust estimation of background noise and signal detection in climatic time series. *Climatic Change*, *33*(3), 409–445. https://doi.org/10.1007/BF00142586

McPhaden, M. J., Zebiak, S. E., & Glantz, M. H. (2006). ENSO as an integrating concept in Earth science. *Science*, *314*(5806), 1740–1745. https://doi.org/10.1126/science.1132588

Mu, M., & Duan, W. (2003). A new approach to studying ENSO predictability: Conditional nonlinear optimal perturbation. *Chinese Science Bulletin*, *48*(10), 1045–1047. https://doi.org/10.1007/s13398-014-0173-7.2

Münnich, M., Cane, M. A., & Zebiak, S. E. (1991). A study of self-excited oscillations of the tropical ocean–atmosphere system. Part II: Nonlinear cases. *Journal of the Atmospheric Sciences*, *48*, 1238–1248.

Newman, M., & Sardeshmukh, P. D. (2017). Are we near the predictability limit of tropical Indo-Pacific sea surface temperatures? *Geophysical Research Letters*, *44*, 8520–8529. https://doi.org/10.1002/2017GL074088

Penland, C., & Sardeshmukh, P. D. (1995). The optimal-growth of tropical sea-surface temperature anomalies. *Journal of Climate*, *8*(8), 1999–2024. https://doi.org/10.1175/1520-0442(1995)008<1999:TOGOTS>2.0.CO;2

Philander, S. G. H. (1990). *El Niño, La Niña, and the Southern Oscillation*. London: Academic Press.

Rasmusson, E. M., & Carpenter, T. H. (1982). Variations in tropical sea surface temperature and surface wind fields associated with the Southern Oscillation/El Niño. *Monthly Weather Review*, *110*(5), 354–384. https://doi.org/10.1175/1520-0493(1982)110<0354:VITSST>2.0.CO;2

Ropelewski, C. F., & Halpert, M. S. (1989). Precipitation patterns associated with the high index phase of the Southern Oscillation. *Journal of Climate*, *2*(3), 268–284. https://doi.org/10.1175/1520-0442(1989)002<0268:PPAWTH>2.0.CO;2

Stein, K., Timmermann, A., Schneider, N., Jin, F. F., & Stuecker, M. F. (2014). ENSO seasonal synchronization theory. *Journal of Climate*, *27*(14), 5285–5310. https://doi.org/10.1175/JCLI-D-13-00525.1

Tang, Y., & Deng, Z. (2010). Low-dimensional nonlinearity of ENSO and its impact on predictability. *Physica D: Nonlinear Phenomena*, *239*(5), 258–268. https://doi.org/10.1016/j.physd.2009.11.006

Tang, Y., & Deng, Z. (2011). Bred vector and ENSO predictability in a hybrid coupled model during the period 1881–2000. *Journal of Climate*, *24*(1), 298–314. https://doi.org/10.1175/2010JCLI3491.1

Tang, Y., Lin, H., & Moore, A. M. (2008). Measuring the potential predictability of ensemble climate predictions. *Journal of Geophysical Research*, *113*, D04108. https://doi.org/10.1029/2007JD008804

Thompson, C. J., & Battisti, D. S. (2000). A linear stochastic dynamical model of ENSO. Part I: Model development. *Journal of Climate*, *13*(4), 2818–2832. https://doi.org/10.1175/1520-0442(2001)014<0445:ALSDMO>2.0.CO;2

Timmermann, A., & Jin, F. F. (2002). A nonlinear mechanism for decadal El Niño amplitude changes. *Geophysical Research Letters*, *29*(1), 1003. https://doi.org/10.1029/2001GL013369

Trenberth, K. E., Branstator, G. W., Karoly, D., Kumar, A., Lau, N. C., & Ropelewski, C. (1998). Progress during TOGA in understanding and modeling global teleconnections associated with tropical sea surface temperatures. *Journal of Geophysical Research*, *103*(C7), 14,291–14,324. https://doi.org/10.1029/97JC01444

Wang, B., Lee, J. Y., Kang, I. S., Shukla, J., Park, C. K., Kumar, A., & Yamagata, T. (2009). Advance and prospectus of seasonal prediction: Assessment of the APCC/CliPAS 14-model ensemble retrospective seasonal prediction (1980–2004). *Climate Dynamics*, *33*(1), 93–117. https://doi.org/10.1007/s00382-008-0460-0

Wang, C., Deser, C., Yu, J.-Y., DiNezio, P., & Clement, A. (2016). El Niño-Southern Oscillation (ENSO): A review. In P. Glymn, D. Manzello, & I. Enochs (Eds.), *Coral reefs of the eastern Pacific* (pp. 85–106). Berlin: Springer Science Publisher.

Wittenberg, A. T. (2009). Are historical records sufficient to constrain ENSO simulations? *Geophysical Research Letters*, *36*, L12702. https://doi.org/10.1029/2009gl038710

Wittenberg, A. T., Rosati, A., Delworth, T. L., Vecchi, G. A., & Zeng, F. (2014). ENSO modulation: Is it decadally predictable? *Journal of Climate*, *27*(7), 2667–2681. https://doi.org/10.1175/JCLI-D-13-00577.1

Wittenberg, A. T., Rosati, A., Lau, N. C., & Ploshay, J. J. (2006). GFDL's CM2 global coupled climate models. Part III: Tropical pacific climate and ENSO. *Journal of Climate*, *19*(5), 698–722. https://doi.org/10.1175/Jcli3631.1

Yu, Y., Duan, W., Xu, H., & Mu, M. (2009). Dynamics of nonlinear error growth and season-dependent predictability of El Niño events in the Zebiak–Cane model. *Quarterly Journal of the Royal Meteorological Society*, *135*(645), 2146–2160. https://doi.org/10.1002/qj.526

Zebiak, S. E., & Cane, M. A. (1987). A model El Niño–Southern Oscillation. *Monthly Weather Review*, *115*(10), 2262–2278. https://doi.org/10.1175/1520-0493(1987)115<2262:AMENO>2.0.CO;2